

# Stopping power of antiprotons in H, H<sub>2</sub>, and He targets

Armin Lühr and Alejandro Saenz

*Institut für Physik, AG Moderne Optik, Humboldt-Universität zu Berlin, Hausvogteiplatz 5-7, D-10117 Berlin, Germany.*

(Dated: November 13, 2018)

The stopping power of antiprotons in atomic and molecular hydrogen as well as helium was calculated in an impact-energy range from 1 keV to 6.4 MeV. In the case of H<sub>2</sub> and He the targets were described with a single-active electron model centered on the target. The collision process was treated with the close-coupling formulation of the impact-parameter method. An extensive comparison of the present results with theoretical and experimental literature data was performed in order to evaluate which of the partly disagreeing theoretical and experimental data are most reliable. Furthermore, the size of the corrections to the first-order stopping number, the average energy transferred to the target electrons, and the relative importance of the excitation and the ionization process for the energy loss of the projectile was determined. Finally, the stopping power of the H, H<sub>2</sub>, and He targets were directly compared revealing specific similarities and differences of the three targets.

PACS numbers: 25.43.+t, 34.50.Bw

## I. INTRODUCTION

During the last two decades low-energy antiproton ( $\bar{p}$ ) collisions have evolved from an exotic system into a powerful tool to achieve understanding of fundamental processes in atoms, molecules, and solids. Obvious advantages of  $\bar{p}$  are that they have a negative charge and are heavy in comparison with an electron and thus ideal projectiles from a theoretical point of view. A number of theoretical efforts have been done, e.g., for low-energy collisions with He atoms focusing on the single and double ionization cross sections. They were stimulated by discrepancies between experiment and theory lasting for more than a decade which only recently could partly be resolved [1]. In the case of ionization and excitation of the simplest two-electron molecule H<sub>2</sub> by  $\bar{p}$  impact the rather sparse information [2, 3] could be extended recently [4]. Precise data on  $\bar{p} + \text{H}_2$  are, however, of great interest in many fields. They can also be used to determine the stopping power which is needed in several applications. It is a prerequisite for the design of low-energy  $\bar{p}$  storage rings taking the interactions with residual-gas atoms and molecules into account. But also the maximum of the stopping power is of importance for the preparation of accurate (future) experiments with low-energy  $\bar{p}$  which are dealing with, e.g., antiprotonic atoms and therefore the capture and annihilation process of  $\bar{p}$ , inelastic scattering events, or the formation of antihydrogen. These experiments are intended to shed more light on fundamental questions regarding the matter-antimatter interaction like tests of the CPT invariance and measurements of the gravity of antimatter. The outcome of collision experiments with  $\bar{p}$  can in turn be used as a stringent test of competing theoretical approaches.

The quantum mechanical formulation of the energy loss of fast charged particles in matter is based on the theory by Bethe [5, 6]. He derived the stopping power in the first-order Born approximation which is propor-

tional to the projectile charge squared  $Z_p^2$ . In Bethe's model, the stopping power  $-dE/dx$  or energy loss per unit length of a charged particle with the velocity  $v$  can be written as

$$-\frac{dE}{dx} = NS(v) = N \frac{4\pi e^4 Z Z_p^2}{m v^2} L(v), \quad (1)$$

where  $N$  is the density of atoms of atomic number  $Z$  in the stopping medium,  $m$  is the electron mass, and  $e$  is the elementary charge.  $S(v)$  is the stopping cross section (related to the stopping power by  $N$ ) and  $L(v)$  is the velocity-dependent stopping number.

While Eq. (1) which is quadratic in  $Z_p$  works sufficiently well for high non-relativistic velocities it was a surprise when it was found in an experiment that the range of negative pions was longer than that of positive pions of equal momentum. The existence of this phenomenon was later fully confirmed with negative and positive hyperons by Barkas *et al.* [7]. This so-called Barkas effect has been interpreted as a polarization effect in the stopping material depending on the charge of the projectile. It appears as the second term in the implied Born expansion of the energy loss and is proportional to  $Z_p^3$ . Following Lindhard [8], the stopping number may be expanded in a Born series in  $Z_p$  as

$$L(v) = \sum_{i=0}^{\infty} Z_p^i L_i(v). \quad (2)$$

where  $L_0$  ( $S \propto Z_p^2$ ) is the Bethe term. The second term  $L_1$  ( $S \propto Z_p^3$ ) also referred to as Barkas correction is the first odd-order term in the Born series and reflects the asymmetry of the energy loss between charge conjugated particles.

With the advent of the Low-Energy Antiproton Ring (LEAR) at CERN,  $\bar{p}$  beams with improved quality at low energy became available, making an accurate comparison of stopping powers for antiprotons and protons ( $p$ ) feasible. The first measurements were performed for solid

silicon [9]. The  $\bar{p}$  stopping powers  $S^{\bar{p}}$  for various solid targets which were obtained in more recent experiments [10] at the Antiproton Decelerator (AD) were found to be smaller by 35-55% than those for  $p$  collisions and confirmed therefore an asymmetry between charge conjugated projectiles. These measurements also strongly supported a proportionality of the stopping power to the velocity below the stopping maximum expected for a point-like projectile.

Stopping powers for  $\bar{p}$  in  $\text{H}_2$  and He were measured by the OBELIX Collaboration [11, 12] also at LEAR for a kinetic energy range of the  $\bar{p}$  from about 0.5 keV to 1.1 MeV. In these experiments, a focus was put on the investigation of the Barkas effect. Their results indicate fundamental differences — calling for a thorough investigation of the involved stopping mechanism — between  $\bar{p}$  stoppings in the simplest gases (He,  $\text{H}_2$ ) and in solid targets below some MeV [12–14]. Particularly, below the  $\bar{p}$  stopping-power maximum no velocity proportionality could be observed. Above the maximum the stopping power  $S^{\bar{p}}$  for  $\bar{p}$  collisions was claimed to be even larger than for  $p$  impact ( $S^p$ ) with a difference  $S^{\bar{p}} - S^p$  of 21%  $\pm 3\%$  and 15%  $\pm 5\%$  around a kinetic energy of 600 keV for  $\text{H}_2$  [13] and 700 keV for He [14], respectively. In a very recent effort [15] the measured He data [12] were reconsidered. After an extended analysis of the data it was claimed that a part of the antiprotons have to be reflected by the wall of the gas vessel in order to bring the simulated results in accordance with the experimentally measured data. A sizeable influence of this newly considered reflection process on the previously analyzed stopping power is, however, not expected by these authors [16]. Although the data were taken more than a decade ago theoretical investigations have not been able to fully reproduce the experimental findings concerning the slowing down of the antiprotons; especially for  $\text{H}_2$  targets.

Approximately at the same time experiments for negatively charged muons ( $\mu^-$ ) stopping in  $\text{H}_2$  and He gases were performed at the PSI [17–19]. In these experiments basically the excitation cross sections were determined by measuring the time-distribution of the scintillation light emitted from the excited targets during the slowing down of the projectile. In order to derive the  $S^{\mu^-}$  also experimental  $\bar{p}$  ionization cross sections and experimental and theoretical data for the mean energy transfer for ionization and excitation of the target were used. In contrast to the  $\bar{p}$  results the  $S^{\mu^-}$  were found to stay below  $S^p$  for energies above the stopping maximum  $E > E_{\text{max}}$ . However, the analysis of the  $\mu^-$  data it was assumed that for fast particles with a velocity  $v \geq 0.1c$  (corresponding to a antiproton energy of approximately 4.7 MeV) the Bethe-Bloch stopping formula is valid. In a more recent measurement for  $\mu^-$  in an  $\text{H}_2$  gas target performed by the same authors the stopping power was measured directly [20]. The results also stay below the proton stopping power for  $E > E_{\text{max}}$ . Although the uncertainties of the latter experiment are considerably larger those in [17–

19] (and thus its results are not discussed quantitatively here) these uncertainties are caused by totally different systematic errors than in the earlier muon experiments providing therefore results which are independent of the earlier findings.

Except for deviations at small projectile velocities  $v$  the total  $\bar{p}$  and  $\mu^-$  stopping powers should be the same at a given  $v$ ,  $S^{\mu^-}(v) = S^{\bar{p}}(v)$ . The deviations among the experimental results are, however, of the order of 20% indicating the experimental difficulties and uncertainties.

A peculiarity in the context of antiproton scattering and in particular for the stopping power is the fact that in the case of hydrogen targets all experiments were done for *molecules* while the theoretical description on the other hand concentrates mainly on *atomic* targets [21–24]. The evident deviations between the theoretical atomic and experimental molecular hydrogen results for  $S^{\bar{p}}$  were therefore claimed to origin from molecular effects [21–23]. The naive picture of an  $\text{H}_2$  molecule as being basically the same as two individual H atoms has been shown to be inadequate for the type of collision processes considered here [4]. It is one aim of the present work to treat the *atomic* and *molecular* hydrogen targets separately in order to figure out the differences and also to compare directly to the experimental findings. The  $\text{H}_2$  molecule and the He atom are described with an effective one-electron model potential which was discussed in detail in [25] and already applied for the determination of ionization and excitation cross sections for  $\bar{p} + \text{H}_2$  collisions [4]. Also, the incongruity among the experimental results is discussed in view of the present findings. Possible deficiencies of the used model description in connection to the stopping power are discussed using the He target which is studied more rigorously theoretically as well as experimentally.

The following section gives a short review on the coupled-channel method applied to the energy-loss calculations and the employed model potential for the target description. In Sec. III the present stopping powers for H,  $\text{H}_2$ , and He are presented and compared to literature. A more detailed discussion of the results follows in Sec. IV. This includes the determination of the Barkas effect and the consideration of the discrepancies among the stopping powers available in literature. Section V concludes on the findings and gives a short outlook. Atomic units are used unless stated otherwise.

## II. METHOD

It can be assumed that the total stopping power of a heavy particle consists of an electronic and a nuclear part. The nuclear stopping power is of importance for very small impact velocities. For  $\bar{p}$  collisions with  $E > 10$  keV it is, however, fully dominated by the electronic stopping power for hydrogen and helium targets [21–23, 26]. In what follows, only the electronic part of the stopping power  $S$  is determined.

A natural approach to measure the stopping power of a medium is to quantify the energy difference of the projectiles before and behind the target medium of a certain thickness and density which may be variable. Instead of looking at the energy which is lost by the projectile it is on the other hand also possible to consider the energy gain of the stopping medium due to the interaction with the projectile. Both perspectives are equivalent since the sum of the energy loss by the projectile and the energy gain by the medium has to be zero. In the present investigation the latter point of view is used to determine the stopping power

$$S = \sum_f (\epsilon_f - \epsilon_i) \sigma_f, \quad (3)$$

where  $\sigma_f$  is the cross section for a transition from the initial state  $i$  into a final state  $f$ . Accordingly,  $\epsilon_i$  and  $\epsilon_f$  are the energies of the states  $i$  and  $f$ , respectively. They express the energy transfer from the projectile to the target needed for the transition and therefore the energy which is lost by the projectile.

In order to obtain the electronic stopping power a general, non-perturbative method for calculating ion collisions is used which has been implemented recently [4, 27]. It is based on a close-coupling approach within an atomic-orbital description of the electrons of the individual target atoms in the stopping medium. An advantage of this approach is the fact that within the space spanned by the basis functions used for the expansion of the time-dependent scattering wave function the projectile-target interaction is treated in infinitely high order. In recent applications ionization and excitation cross sections as well as electron-energy spectra were determined for antiproton and proton collisions with alkali-metal atoms [27, 28] and molecular hydrogen [4, 25, 29].

The collision process is considered in a semi-classical way using the impact parameter method. Thereby, the target electrons are treated quantum mechanically while the heavy projectile moves on a straight classical trajectory  $\mathbf{R}(t) = \mathbf{b} + \mathbf{v}t$  given by the impact parameter  $\mathbf{b}$  and the velocity  $\mathbf{v}$  which are parallel to the  $x$  and  $z$  axis, respectively, and  $t$  is the time.

An effective one-electron description of the collision process is used,

$$i \frac{\partial}{\partial t} \Psi(\mathbf{r}, \mathbf{R}(t)) = \left( \hat{H}_0 + \hat{V}_{\text{int}}(\mathbf{r}, \mathbf{R}(t)) \right) \Psi(\mathbf{r}, \mathbf{R}(t)), \quad (4)$$

where  $\mathbf{r}$  is the electron coordinate and the interaction between the projectile with charge  $Z_p$  and the target electron is expressed by the time-dependent interaction potential

$$\hat{V}_{\text{int}}(\mathbf{r}, \mathbf{R}(t)) = -\frac{Z_p}{|\mathbf{r} - \mathbf{R}(t)|}. \quad (5)$$

The time-dependent scattering wave function

$$\Psi(\mathbf{r}, \mathbf{R}(t)) = \sum_j c_j(\mathbf{R}(t)) \phi_j(\mathbf{r}) \quad (6)$$

is expanded in eigenstates  $\phi_j$  of the time-independent target Hamiltonian

$$\hat{H}_0 = -\frac{1}{2} \nabla^2 + \hat{V}_{\text{target}}(r). \quad (7)$$

The  $\phi_j$  are centered on the target nucleus. Their radial part is expanded in B-spline functions while their angular part is expressed in spherical harmonics.

The potential  $V_{\text{target}}$  in Eq. (7)

$$V_{\text{target}}(r) = -\frac{1}{r} \left( 1 + \frac{\alpha}{|\alpha|} \exp \left[ -\frac{2r}{|\alpha|^{1/2}} \right] \right), \quad (8)$$

used for the (effective) one-electron description of the target was proposed in [30] and discussed in detail in [25]. The potential in Eq. (8) becomes parameter free by requiring  $\alpha$  to be chosen in such a way that the ionization potential of the model coincides with the one of the target. Additionally, in the limit  $\alpha \rightarrow 0$  one obtains the potential for atomic hydrogen  $V_{\text{target}}(r) = V_{\text{H}}(r) = -1/r$  as well as in the limit  $r \rightarrow 0$  for arbitrary  $\alpha$ . A value of  $\alpha = 0.8791$  yields the correct ionization potential for ground state He atoms. In the case of an  $\text{H}_2$  molecule one has to keep in mind that the ionization potential is — in a fixed nuclei approximation — dependent on the internuclear distance  $R_n$  between the two nuclei. The relation between  $R_n$  and  $\alpha$  is given in [25].

It has been shown in [4] that within the Born-Oppenheimer approximation cross sections for antiproton collisions with  $\text{H}_2$  are linear in  $R_n$  around  $R_n = 1.4$  a.u. This property was used according to [31] in order to obtain cross sections which are independent of  $R_n$  and to a certain extent also account for the motion of the  $\text{H}_2$  nuclei. However, the rovibronic motion is due to the use of closure energetically not resolved. The procedure used here employs closure, exploits the linear behavior in  $R_n$  of the cross section around  $R_n = 1.4$  a.u., and finally performs the calculations at  $R_n = \langle R_n \rangle = 1.4487$  a.u. Therefore, the value  $\alpha = 0.13308$  is used in the present calculations which results in an ionization potential of the model which is equal to the ionization potential of  $\text{H}_2$  for  $R_n = \langle R_n \rangle = 1.4487$  a.u.

The expansion of  $\Psi(\mathbf{r}, \mathbf{R}(t))$  in Eq. (4) as given in Eq. (6) leads to coupled, first-order differential equations for the expansion coefficients  $c_j(\mathbf{R}(t))$  for every trajectory  $\mathbf{R}(t)$ , i.e., for every  $v$  (and therefore for every impact energy  $E = (1/2) M_p v^2$  where  $M_p$  is the projectile mass) and  $b$ . The differential equations are integrated in a finite  $z$  range  $-40$  a.u.  $\leq z = vt \leq 70$  a.u. with the initial condition  $c_j(\mathbf{R}(t_i = -40/v)) = \delta_{ji}$  that the target is initially in its ground state  $\phi_i$ .

The single-electron probability for a transition into the final state  $\phi_f$  at  $t_f = 70/v$  is given by

$$p_f(b, v) = |c_f(b, v, t_f)|^2 \quad (9)$$

and is used for H atoms. In the case of the two-electron targets  $\text{H}_2$  and He the independent particle model (IPM) is employed. It assumes that both electrons have the

same transition probabilities which are simply given by the single-electron probabilities Eq. (9). Furthermore, the electrons are considered as being independent of each other in the way that both feel the same attractive potential  $V_{\text{target}}$  which includes the interaction with the other electron only by an averaged screening of the nuclear charge. As a consequence the total stopping power due to one electron is—in contrast to the cross sections obtained with the IPM— independent from and equal to the one of the other electron. Therefore, in the case of targets with  $N$  electrons the final stopping power given in Eq. (3) computed for a single electron by using Eq. (9) has to be multiplied with the factor  $N$  in order to sum up the contributions from all  $N$  independent electrons.

This argument can also be expressed in a more formal way starting with the relation

$$1 = \sum_j p_j = \sum_j p_j \sum_k p_k = \sum_{j,k} p_j p_k, \quad (10)$$

where it has been used that the sum over all single-electron transition probabilities  $p_j$  including the probability for staying in the initial state is unity. The indices  $j$  and  $k$  are meant to indicate one of the electrons. Actually, the transition probabilities all depend on  $b$  and  $v$  which is for the sake of clarity not explicitly written in this derivation. In view of the stopping power (cf. Eq. (3)) the transition probabilities in Eq. (10) are multiplied with the sum of energies  $\tilde{\epsilon}_j + \tilde{\epsilon}_k$  needed for the transitions of one electron into state  $\phi_j$  and the other into  $\phi_k$

$$\sum_{j,k} p_j p_k (\tilde{\epsilon}_j + \tilde{\epsilon}_k) = \sum_{j,k} p_j p_k \tilde{\epsilon}_j + \sum_{j,k} p_j p_k \tilde{\epsilon}_k \quad (11)$$

$$= 2 \sum_{j,k} p_j p_k \tilde{\epsilon}_j \quad (12)$$

$$= 2 \sum_j p_j \tilde{\epsilon}_j \underbrace{\sum_k p_k}_{=1} \quad (13)$$

$$= 2 \sum_j p_j \tilde{\epsilon}_j = \sum_j p_j (2\tilde{\epsilon}_j). \quad (14)$$

It should be noted that the use of the sum of single-electron energies for both electrons is an approximation which seems, however, to be consistent within the employed IPM. This approximation is reasonable if one-electron transitions are dominating the electronic energy loss. Finally, the last line can be interpreted in the way that the total single-electron stopping power is multiplied with a factor two which accounts for both electrons as mentioned above. Note, that the sum of all probabilities is still unity and is therefore conserved as it should be.

A similar derivation as in Eqs. (11–14) can be used in the case that the summation runs only over a limited number of final states. As an example the contribution to the stopping power due to double ionization shall be considered. Then the indices  $j$  and  $k$  only take continuum states into account leading to a restricted summation indicated by an asterisk above the sum. Equations (12–14)

then take the form

$$2 \sum_{j,k}^* p_j p_k \tilde{\epsilon}_j = 2 \sum_k^* p_k \sum_j^* p_j \tilde{\epsilon}_j \quad (15)$$

$$= 2 p_I \sum_j^* p_j \tilde{\epsilon}_j, \quad (16)$$

where  $p_I$  is the sum of all single-electron transition probabilities into continuum states.

The contribution to the stopping power from all electron transitions into the continuum is obtained by relaxing the restriction on the sum over  $k$  in Eq. (15) to all possible final states of the other electron

$$2 \sum_k \sum_j^* p_j p_k \tilde{\epsilon}_j = 2 \sum_k p_k \sum_j^* p_j \tilde{\epsilon}_j = 2 \sum_j^* p_j \tilde{\epsilon}_j, \quad (17)$$

which yields a factor one instead of  $p_I$  in Eq. (16). Thus, the same result as in the one-electron case is obtained which is just multiplied with a factor two. However, in the case of two-electron targets this is the sum of contributions due to single and double ionization. Accordingly, the contribution to the stopping power from all electron transitions into bound states is given by

$$2 \sum_k \sum_j^{\bar{}} p_j p_k \tilde{\epsilon}_j = 2 \sum_k p_k \sum_j^{\bar{}} p_j \tilde{\epsilon}_j = 2 \sum_j^{\bar{}} p_j \tilde{\epsilon}_j, \quad (18)$$

where the bar above the sum indicates that the summation is restricted to bound states only. The sum of the contributions due to ionization (Eq. (17)) and excitation (Eq. (18)) obviously yields the correct total result as given in Eq. (14).

The results in Eqs. (14–18) for the stopping power seem to contradict with the way how two-electron cross sections are extracted from single-electron probabilities employing the IPM. For cross sections it is important that the probability for double excitation (or ionization) is only counted once and not twice in order to preserve the sum of probabilities being unity. The factor two in the case of the stopping power, however, appears not due to an increase of the probability for double transitions but because of the fact that in these transitions both electrons gain energy and the probability has therefore to be weighted with the number of electrons by what the seeming contradiction is resolved.

The cross section  $\sigma_f$  required for the determination of the total stopping power in Eq. (3) for a certain  $v$  is obtained (using the cylindrical symmetry of the collision system) by an integration over  $b$ ,

$$\sigma_f(v) = 2\pi \int p_f(b, v) b db, \quad (19)$$

where  $p_f$  is given in Eq. (9). In the case of two-electron targets the result obtained with Eq. (3) has to be multiplied—in accordance with Eq. (14)— with the factor two.

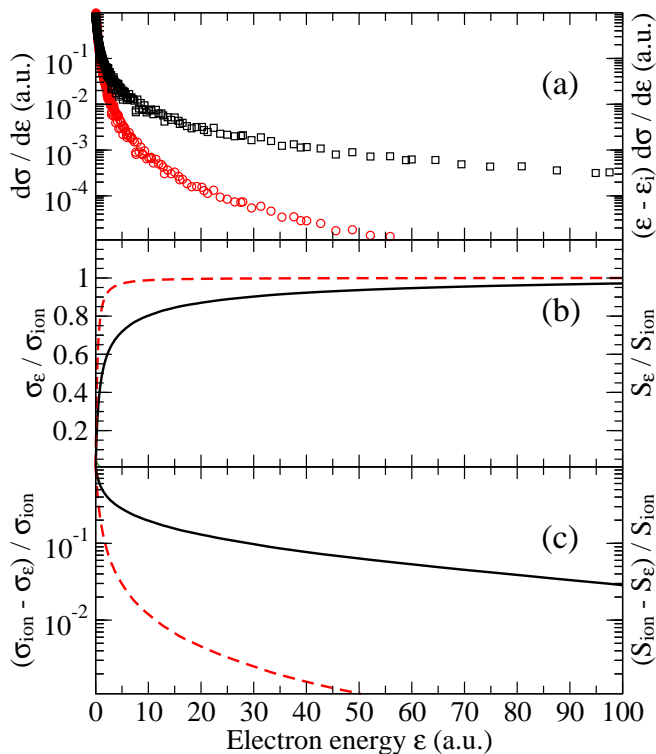


Figure 1: (Color online) Convergence behavior of the ionization cross section and the contribution to the stopping power caused by ionization with respect to the energy cutoff of the basis. The results are given for 3.2 MeV antiproton collisions with  $\text{H}_2$ . (a) Electron energy spectrum  $d\sigma/d\epsilon$ , red circles; electron energy spectrum multiplied with the energy required for the excitation  $(\epsilon - \epsilon_i) d\sigma/d\epsilon$  (see Eq. (3)), black squares. (b) Ratio  $\sigma_\epsilon/\sigma_{\text{ion}}$  of the ionization cross sections with an energy cutoff  $\epsilon$  to the one with the cutoff 250 a.u., red dashed line; ratio  $S_\epsilon/S_{\text{ion}}$  of the stopping power caused by ionization with an energy cutoff  $\epsilon$  to the one with the cutoff 250 a.u., black solid line. (c) The deviation from unity of the curves given in (b).

The present results were calculated with a basis set similar to that used in [27] including orbitals with angular momenta up to  $l = 7$ . An energy cutoff for the continuum states of 250 a.u. was used leading to about 260 B-spline functions per angular momentum. A non-linear knot sequence was employed for the radial coordinate. The interaction potential in Eq. (5) causes  $l$  and  $m_l$  mixing. In order to reduce the numerical effort only orbitals with magnetic quantum numbers  $|m_l| \leq 3$  were taken into account. Exploiting the symmetries of the collision system  $\Psi$  was expanded in a total number of 6540 states. All parameters given above were checked thoroughly in convergence tests.

It was found that especially a sufficiently high energy cutoff and density of continuum states also at large state energies are of importance for converged results. This is somehow contrary to what is expected for ionization cross sections. However, an insufficient choice of both

parameters influences the final stopping power differently which may even lead to some kind of compensation. A too small energy cutoff results in a too small stopping power while an improvement of the density of continuum states, on the other hand, led in the present study to smaller stopping powers.

Figure 1 illustrates the convergence with respect to the energy cutoff of the employed basis of the contribution to the stopping power caused by ionization  $S_{\text{ion}}$  (cf. Eq. (17)) and the ionization cross section  $\sigma_{\text{ion}}$ . The results are calculated for 3.2 MeV antiprotons colliding with  $\text{H}_2$ . In Fig. 1(a) it can be seen that the electron energy spectrum  $d\sigma/d\epsilon$  decreases much faster for increasing  $\epsilon$  than the product  $(\epsilon - \epsilon_i)d\sigma/d\epsilon$ . Therefore, the contribution to the stopping power caused by ionization converges much slower with respect to the cutoff energy of the basis than the ionization cross section, as can be seen in Fig. 1(b). Here, the quantities  $\sigma_\epsilon$  and  $S_\epsilon$  only take transitions into final states  $\phi_f$  with positive  $\epsilon_f \leq \epsilon$  into account. Figure 1(c) shows how much  $\sigma_\epsilon$  and  $S_\epsilon$  deviate from the final value ( $\epsilon_f \leq 250$  a.u.) when the cutoff energy is chosen as  $\epsilon$ . In table I those cutoff energies are given which recover the final values of  $\sigma_{\text{ion}}$  and  $S_{\text{ion}}$  obtained with a cutoff of 250 a.u. within 90, 95, 97, and 99%. Figure 1(c) and table I clearly show the different convergence behavior of  $\sigma_\epsilon$  and  $S_\epsilon$  with respect to the cutoff energy. While the ionization cross section is converged within approximately 1% with a cutoff of 10 a.u. in the case of  $S_{\text{ion}}$  a convergence within 3% is only achieved with an cutoff of around 100 a.u.

Obviously, this slow convergence behavior of  $S_{\text{ion}}$  becomes more pronounced for higher impact energies since the relative population of high-lying continuum states increases leading to a less steep fall-off of the electron energy spectra as it was discussed in [4]. On the other hand, for lower impact energies a smaller energy cutoff is sufficient since the electron energy spectra fall off steeply for  $\epsilon \geq \frac{1}{2}(2v)^2$  corresponding to the maximally transferred energy in a classical collision [4].

Table I: Convergence with respect to the energy cutoff of the ionization cross section  $\sigma_{\text{ion}}$  and the contribution to the stopping power caused by ionization  $S_{\text{ion}}$  for 3.2 MeV antiproton collisions with  $\text{H}_2$ . Four different values for the energy cutoff are given which are sufficient to recover the final result (with an cutoff energy of 250 a.u.) within the given relative accuracy.

degree of recovery of final value (%)	energy cutoff $\epsilon$ (a.u.)	
	$\sigma_{\text{ion}}$ (a.u.)	$S_{\text{ion}}$ (a.u.)
90	1.8	29.0
95	3.2	63.5
97	4.8	96.5
99	11.3	155

### III. RESULTS

Calculations were performed for  $\bar{p}$  collisions with the three targets H, H<sub>2</sub>, and He. The present data for the stopping power are listed in Table II. In the following the findings of all three targets will be separately discussed and compared with literature data.

#### A. $\bar{p} + \text{H}$

The stopping power for atomic hydrogen is shown in Fig. 2. Since no experiments have been performed for atomic hydrogen targets so far the present results are compared to various theoretical calculations for  $\bar{p}$  and  $\mu^-$  impact. The stopping power for hydrogen atoms is preferably used for the testing of a theoretical approach since the target description is well known and in principle no approximations are needed. A detailed analysis of  $S$  for H and He was done by Schiwietz *et al.* [21] comparing three different approaches, namely, an atomic-orbital (AO), a distorted-wave (DW), and an adiabatic-ionization (AI) description. Due to the inherent approximations of the AI — adiabatic collision — and the DW — interaction in first order — approaches they are basically low-energy and high-energy methods, respectively. Their advantage over the AO method is based on their comparably small numerical effort. The AI and DW results describe the stopping power reasonably for  $E < 20$

Table II: Stopping power  $S$  per atom for antiproton collisions with H, H<sub>2</sub>, and He in  $10^{-15}$  eV cm<sup>2</sup> / atom which are shown in Figs. 2, 3, and 4, respectively. The results for H<sub>2</sub> are given for the mean value of the internuclear distance  $R_n = \langle R_n \rangle = 1.4487$  a.u. as proposed in [4].

$E$ (keV)	H	H <sub>2</sub>	He
1	2.774	2.242	2.261
2	3.164	2.503	2.524
4	3.641	2.826	2.859
8	4.208	3.188	3.280
16	4.782	3.596	3.795
25	5.098	3.831	4.144
32	5.196	3.947	4.367
50	5.210	4.027	4.666
64	5.115	4.013	4.811
100	4.623	3.782	4.850
128	4.229	3.557	4.753
200	3.406	2.950	4.316
256	2.938	2.588	3.965
400	2.148	1.961	3.202
800	1.239	1.165	2.036
1600	0.681	0.656	1.189
3200	0.361	0.356	0.668
6400	0.187	0.187	0.358

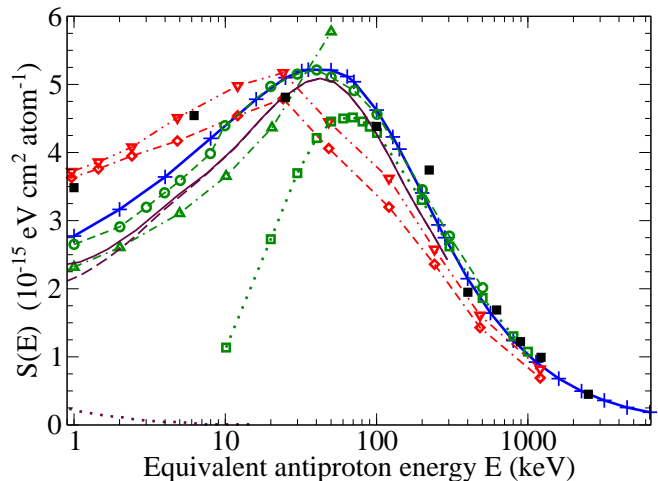


Figure 2: (Color online) Energy-loss cross section  $S(E)$  for H targets as a function of the equivalent antiproton impact energy  $E$ . **Theory.** Present results: blue solid curve with plus. Schiwietz *et al.* [21]: green dashed curve with circles, atomic orbital (AO); green dash-dotted curve with triangles up, adiabatic-ionization (AI); green dotted curve with squares, distorted wave (DW). Cabrera-Trujillo *et al.* [22]: brown thin solid curve, total  $S$ ; brown long dashed curve, electronic  $S$ ; brown dotted curve, nuclear  $S$ . Custidiano and Jakas [23]: black squares, CTMC for  $\bar{p}$ . Cohen [24]: red dash-doubly-dotted curve with triangles down, CTMC (CL) for  $\mu^-$ ; red doubly-dash-dotted curve with diamonds, quantum-classical CTMC (QC) for  $\mu^-$ .

keV and  $E > 100$  keV, respectively. Note, that the use of the DW method leads to a clearly different position and height of the stopping maximum compared to the AO method and the AI curve does not show any maximum at all. The present findings, which are also based on an atomic-orbital approach, are in good agreement with the AO results, except for the regime  $2 \text{ keV} < E < 8 \text{ keV}$  where a small discrepancy exists. From the comparison to the AO results it is assumed that the present method is correctly implemented.

Cabrera-Trujillo *et al.* [22] employed the electron-nuclear dynamics (END) theory which is based on the application of the time-dependent variational principle to the Schrödinger equation using a coherent state representation of the wave function. This method allows for the simultaneous determination of the electronic and nuclear stopping power. The latter is small for all surveyed projectile energies and completely negligible for  $E > 10$  keV. The END results for the electronic stopping power show a similar behavior like both AO calculations but predict throughout lower values. These three curves share in particular the position of the maximum at around  $E_{\text{max}} \approx 40$  keV and similar slopes for energies below and above  $E_{\text{max}}$ .

The Classical Trajectory Monte Carlo (CTMC) method was recently employed by Custidiano and Jakas [23] in order to determine  $S^{\bar{p}}$  and earlier already by Co-

hen [24] for  $S^{\mu^-}$ . Both calculations agree for high energies  $E > 200$  keV with the AO, DW, and END results but differ from them below the stopping power maximum sharing the same slope. While the CTMC results for  $S^{\bar{p}}$  follow the trend of the AO and END curves down to about 20 keV the  $S^{\mu^-}$  results by Cohen show a different behavior in the energy range around  $E_{\max}$ . Besides the purely classical CTMC (CL) Cohen also provided a quantum-classical analysis (QC) of his data. They differ mainly in the vicinity of  $E_{\max}$  where the CL results are closer to the END and AO curves than those from the QC analysis. It was shown in [23] that for low impact energies  $E < 30$  keV the CTMC stopping power depends considerably on the eccentricity of the initial classical electron orbits. The similar behavior of all CTMC results below 30 keV may be caused by the fact that Custidiano and Jakas followed a procedure for preparing initial conditions described by Cohen.

Finally, it is possible to conclude that the present findings for H targets agree well with the other AO calculation and share the same behavior than the END results. For all other approaches considered here the energy range in which they are applicable is limited to energies around and above the stopping maximum  $E \gtrsim E_{\max}$  except for the AI method which gives reasonable results only below the maximum.

## B. $\bar{p} + \text{H}_2$

In Fig. 3 the  $S(E)$  for  $\text{H}_2$  targets is shown as a function of the equivalent antiproton impact energy. The equivalent antiproton energy can be obtained by multiplication of the impact energy with the factor  $m_{\bar{p}}/M_p$  where  $m_{\bar{p}}$  is the mass of an antiproton. The factor for  $\mu^-$  projectiles is accordingly  $m_{\bar{p}}/m_{\mu^-} \approx 8.880$ . The present data are calculated for a fixed internuclear distance  $R_n = \langle R_n \rangle = 1.4487$  a.u. of the two nuclei as proposed in [4, 31]. The consideration of isotopes of hydrogen molecules leads to a slightly different  $\langle R_n \rangle$  [33]. The effect on the stopping power for different  $R_n$  in the range  $1.4 \text{ a.u.} \leq R_n \leq 1.5 \text{ a.u.}$  is only quantitative and largest around the stopping maximum where the deviation is of the order of 1.5%.

In contrast to the hydrogen atom three experiments have been performed for  $\text{H}_2$  whereas the authors are only aware of a single calculation in the molecular case by Schiwietz *et al.* [21] employing the AI method in which the  $\text{H}_2$  molecule was described in a quasiatomic way with a single effective scaled charge. Within an IPM the effective charge was chosen in such a way that the total electronic energy of the molecule at its equilibrium internuclear distance is reproduced.

It is evident from Fig. 3 that the experimental results for  $S^{\bar{p}}$  by Adamo *et al.* [11] and by Agnello *et al.* [12] as well as for  $S^{\mu^-}$  by Hauser *et al.* [18] all differ considerably. For high energies  $E > 200$  keV the findings for  $\bar{p}$  impact by Adamo *et al.* and  $\mu^-$  impact are very simi-

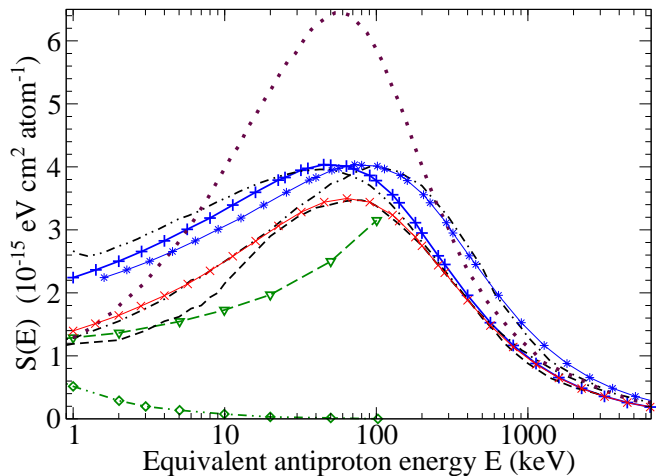


Figure 3: (Color online) Energy-loss cross section  $S(E)$  for  $\text{H}_2$  targets as a function of the equivalent antiproton impact energy  $E$ . **Theory.** Present results: blue solid curve with plus,  $R_n=1.4487$ ; blue thin solid curve with stars,  $E$  scaled by a factor 1.6 (see text); red thin solid curve with x, double ionization excluded (see text). Schiwietz *et al.* [21]: green dashed curve with triangles down, adiabatic-ionization (AI); green dash-doubly-dotted curve with diamonds, nuclear stopping. **Experiment.**  $\bar{p}$ : Agnello *et al.* [12], black dash-dotted curve; Adamo *et al.* [11], black dash-doubly-dotted curve.  $\mu^-$ : Hauser *et al.* [18], black dashed curve.  $p$ : Andersen and Ziegler [32], brown dotted curve.

lar. At energies below the maximum the  $S^{\mu^-}$  are closer to the more recent  $\bar{p}$  results by Agnello *et al.* The maxima of the three experimental curves [11], [12], and [18] are situated approximately at the equivalent antiproton energies  $E_{\max} \approx 45$  keV, 100 keV, and 75 keV, respectively. While the maxima of both  $S^{\bar{p}}$  curves are of comparable height the maximum of  $S^{\mu^-}$  lies well below those two.

It should be noted that the experimental curves shown here are the best fit results from an analysis of the measured data. The order of the uncertainties was estimated in [12] to amount to  $\pm 10\%$ . In the case of the  $\mu^-$  results the uncertainties vary from  $\pm 10\%$  for impact energies in the vicinity and above  $E_{\max}$  and increase up to  $\pm 50\%$  for decreasing  $E$ . Furthermore, in the  $\mu^-$  experiments basically the excitation cross section was determined only as stated already in the introduction. The shown  $S^{\mu^-}$  results depend therefore also on additional data which were taken from literature. The experimental  $\bar{p}$  ionization cross sections  $\sigma_{\text{ion}}$  [34] used in order to determine  $S^{\mu^-}$ , however, were later on found to be erroneous for  $E < 200$  keV [2, 35].

Due to these substantial uncertainties it is one aim of this work to discriminate with the help of the present findings between the different experimental results. For  $E > 200$  keV the present results are in good agreement with the  $\mu^-$  data and the  $S^{\bar{p}}$  by Adamo *et al.* While the latter curve has a similar behavior like the present calculations also in the vicinity and below the maximum

the former  $S^{\mu^-}$  curve deviates clearly for  $E < 200$  keV. The  $S^{\bar{p}}$  curve determined by Agnello *et al.* is on the other hand not compatible with the present data. While the height of both maxima is very similar it appears as if the experimental curve is shifted to larger energies. A simple scaling of  $E$  by a factor of 1.6 between the present and the experimental  $\bar{p}$  data by Agnello *et al.* as proposed in [29] can, however, not be verified in view of the current more detailed investigation. The scaled curve clearly deviates from the measured data for the highest energies. On the other hand, it is the scaled curve which looks most similar to the one for  $S^{\bar{p}}$  by Agnello *et al.* for impact energies around and above the stopping maximum.

It is known that the IPM overestimates the two-electron processes like double ionization (e.g., [36]) which was also observed in an earlier application of the model potential [25]. Single excitation and single ionization are on the other hand reasonably well described. Therefore, the present stopping power without the contribution from double ionization  $S^{\text{sin}}$  has also been analyzed by using the difference between Eq. (14) and Eq. (16) instead of the total  $S$  given by Eq. (14). The qualitative behavior of the present curves for  $S$  and  $S^{\text{sin}}$  is similar due to the fact that both curves originate from the same calculation. The quantitative difference on the other hand increases for low impact energies. While the relative difference is below 1% for  $E > 1500$  keV it is larger than 10% for  $E < 100$  keV and finally becomes as large as one third for  $E = 2$  keV. In the validity range of the used model this curve can be interpreted as a lower bound to the stopping power. For  $E > 40$  keV  $S^{\text{sin}}$  matches the experimental  $S^{\mu^-}$  while for  $E < 25$  keV the experimental data by Agnello *et al.* are reproduced by  $S^{\text{sin}}$ . Unfortunately, the authors are not aware of any independent and reliable data for the single and especially double ionization or excitation cross section for low-energy  $\bar{p} + \text{H}_2$  collisions. These would allow for a quantitative approximation of the uncertainties due to the model potential and the use of the IPM for impact energies below 100 keV.

The other theoretical curve calculated by Schiwietz *et al.* shows a similar dependence on  $E$  like the AI results in the case for atomic H targets. It agrees with the measurements of  $S^{\bar{p}}$  by Agnello *et al.* and of  $S^{\mu^-}$  by Hauser *et al.* for  $E < 5$  keV but differs clearly for  $E > 10$  keV from all other curves. The nuclear stopping power also calculated by Schiwietz *et al.* [21] is again small in the considered energy regime but considerably larger than the END results in the case of atomic H.

A comparison to the stopping power for  $p$  impact shows a maximum at  $E \approx 60$  keV which is about 60% larger than the present value for  $S^{\bar{p}}$ . Note that all curves in Fig. 3 lie below the  $p$  results for energies larger than  $E_{\text{max}}$  except for  $S^{\bar{p}}$  determined by Agnello *et al.* At high energies all curves converge to the  $p$  results showing a  $1/v^2$  dependence of  $S$  as expected from the Bethe theory (cf. Eq. (1)). Below the maximum only the present curve and the one by Adamo *et al.* cross the  $p$  curve for  $E > 1$

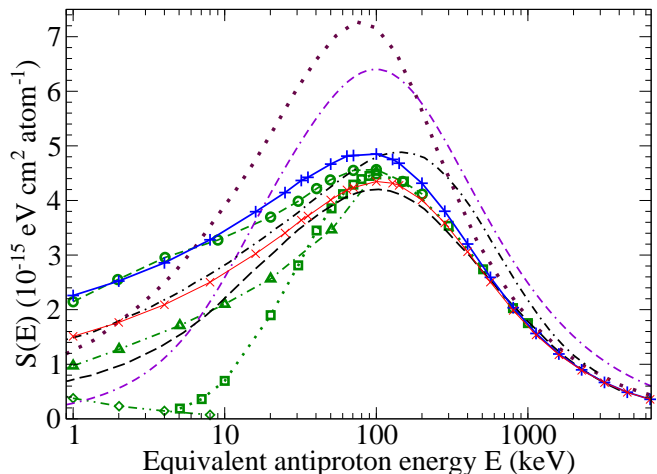


Figure 4: (Color online) Energy-loss cross section  $S(E)$  for He targets as a function of the equivalent antiproton impact energy  $E$ . **Theory.** Present results: blue solid curve with plus; red thin solid curve with x, double ionization excluded (see text). Schiwietz *et al.* [21]: green dashed curve with circles, atomic orbital (AO); green dash-dotted curve with triangles up, adiabatic-ionization (AI); green dotted curve with squares, distorted wave (DW); green dash-doubly-dotted curve with diamonds, nuclear stopping. Basko [37]: violet doubly-dash-dotted curve, low-velocity Bohr (LVB). **Experiment.**  $\bar{p}$ : Agnello *et al.* [12], black dash-dotted curve.  $\mu^-$ : Kottmann [17], black dashed curve.  $p$ : Andersen and Ziegler [32], brown dotted curve.

keV resulting in a change of the sign of the Barkas term.

### C. $\bar{p} + \text{He}$

In contrast to hydrogen, data of more than one experimental and theoretical approach exist for He targets. They are shown in Fig. 4 together with the present findings and the experimental results for  $p$  impact. For  $\bar{p} + \text{He}$  collisions also the ionization cross section  $\sigma_{\text{ion}}$  is experimentally and especially theoretically well studied (cf. [1] and references therein) making it a good candidate for the comparison of different approaches.

The experimental curves for  $\bar{p}$  and  $\mu^-$  stopping in He gases show a behavior similar to the one of the  $\text{H}_2$  target measured by the same groups which were shown in Fig. 3. The stopping maximum is approximately 25% higher for He than for  $\text{H}_2$ . Again the experimental  $S^{\bar{p}}$  by Agnello [12] *et al.* is larger than the  $p$  results by Andersen and Ziegler [32] above the stopping maximum while the measured  $S^{\mu^-}$  by Kottmann [17] stays below the  $p$  curve for all energies considered here.

As for the atomic H target Schiwietz *et al.* [21] applied the AI, AO, and DW method to calculate the He stopping power. The AI curve shows a functional dependence on  $E$  analogous to the one observed for H and  $\text{H}_2$  targets. That is, for small  $E$  it is generally in accordance with



the two experimental  $S^{\bar{p}}$  and  $S^{\mu^-}$  curves while it seems not to be applicable for  $E > 20$  keV. The DW results fully agree with the experimental  $S^{\mu^-}$  for  $E > 300$  keV but fall off much faster below the stopping maximum for  $E < 40$  keV. Exactly the same behavior was observed for  $\sigma_{\text{ion}}$  calculated earlier by Fainstein *et al.* [38] also using a DW method which coincides with the  $\sigma_{\text{ion}}$  resulting from the DW calculations by Schiwietz *et al.* [21]. Although first measurements of low-energy ionization for  $\bar{p} + \text{He}$  collisions [2, 39] fully confirmed this steep fall off below the ionization maximum, a recent more accurate experiment was able to clearly contradict this trend [1] in favor of a less steep decrease of  $\sigma_{\text{ion}}$  below the maximum. The  $S$  results calculated by Schiwietz *et al.* using the AO and the DW method fully agree with each other for  $100 < E < 200$  keV both having a maximum value lying in between the two experimental curves at  $E \approx 100$  keV. This is somehow different from the case of atomic H targets where the height and position of the AO and DW stopping maxima clearly differ (see Fig. 2). Below the maximum, however, the two curves diverge with decreasing  $E$ . The AO results stay above the DW and the experimental data with deviations increasing to more than 50% for  $E < 5$  keV. These deviations of the AO results were explained by the use of a model treating one active electron in the effective potential of the heavy nucleus and a static density distribution of the second inactive electron which screens the nucleus [21]. In the adiabatic limit of the AO model for He no ionization threshold exists for  $R \rightarrow 0$  as it is known for an H atom also referred to as Fermi-Teller radius. This is, however, in contrast to a full two-electron treatment of a He atom which leads for  $R \rightarrow 0$  to a finite ionization threshold of  $\approx 0.7$  eV due to the fact that the electron density is changed dynamically when the  $\bar{p}$  approaches the nucleus. Therefore, the AO results were expected to overestimate the ionization cross section and consequently also the stopping power for low  $E$  [21].

The present results for  $S$  coincide with the experimental  $S^{\mu^-}$  and theoretical DW data for high energies  $E > 500$  keV but become considerably larger for  $E < 200$  keV. Like for the  $\text{H}_2$  target the maximum of the present He curve has the same height as the  $S^{\bar{p}}$  measured by Agnello *et al.* and it is situated around 100 keV as predicted by the AO and DW methods. Below the stopping maximum the present data are, however, much larger than the experimental  $S^{\bar{p}}$  and  $S^{\mu^-}$  and theoretical AI results. The present calculations are, on the other hand, basically in agreement with the AO data for low energies. Therefore, it may be concluded that the deviations of the present findings at low energies also originate from deficiencies of the employed effective one-electron model which lead to substantial changes of the ionization potential in the adiabatic limit as is the case for the AO model. Due to the existing uncertainties of experimental and theoretical results, especially for low energies, it is, however, not possible to finally conclude on the exact behavior of the stopping power in this energy range. On the other

hand, the error of the measured  $S^{\mu^-}$  curve could be reduced drastically if a point at low energies could be fixed safely [17]. In this context it would be valuable to perform a calculation using a full two-electron description of the target to eliminate the uncertainties connected so far with both AO approaches using effective one-electron models.

As has been done for  $\text{H}_2$  the stopping power excluding double ionization  $S^{\text{sin}}$  has also been analyzed for He targets. The present  $S$  and  $S^{\text{sin}}$  curves are again qualitatively similar while quantitative differences increase for lower impact energies. The relative contribution from double ionization to  $S$  is at low energies slightly smaller than in the case of  $\text{H}_2$  while it is the other way round at high energies. It is interesting to note that these relative contributions correspond roughly to the ratios of cross sections for double and single ionization in the IPM (e.g., [36]) multiplied by two. The factor two accounts for the energy of both electrons involved in the double ionization. The  $S^{\text{sin}}$  curve lies above the experimental data for  $\mu^-$  for  $E < 400$  keV indicating that the measured results might be too small. For  $E < 25$  keV  $S^{\text{sin}}$  describes the experimental  $\bar{p}$  data reasonable as it is the case for  $\text{H}_2$  pointing out that the contribution of double ionization in  $S$  is too large especially at low energies.

In contrast to the case of  $\bar{p} + \text{H}_2$  a number of advanced calculations (e.g., [40–42]) were performed for  $\bar{p} + \text{He}$  ionization cross sections in addition to the experiments. This allows for a rough estimate of some of the uncertainties of the present results stemming from the target model and the use of the IPM for the presented He stopping power as well as for an attempt to estimate an corrected value of  $S$  at low impact energies. The present cross section for single ionization is in good agreement with experiment for  $E > 40$  keV but becomes increasingly too large for smaller impact energies due to the reasons discussed above. The cross section for double ionization depends quadratically on the single-electron ionization probability within the IPM which is, however, known to overestimate the measured data (cf., e.g., [36]). In the following, the averaged energy transfer is assumed to be described correctly. Then the stopping power depends linearly on the cross sections. Under this assumption the correct contribution to the stopping power due to double ionization may be roughly approximated as being only 50%, 43%, and 30% of the difference  $S - S_{\text{sin}}$  for the three energies 200, 100, and 25 keV, respectively. The single ionization cross section of a recent accurate calculation [40] is approximately 10% smaller than the present one for  $E = 25$  keV. For this energy a value of the present stopping power which includes all mentioned assumptions and corrections may be therefore roughly approximated with  $3.3 \cdot 10^{-15}$  eV cm<sup>2</sup> per atom. This value lies slightly below the curve for  $S_{\text{sin}}$ . Although no quantitative estimate can be done for  $\text{H}_2$  targets as discussed above it might be expected that the correction is qualitatively similar to that performed for He. Note that the contributions due to excitation have not been

changed in this simple estimate. The above discussion obviously shows the need for further calculations using a two-electron description of the target in order to improve the quantitative description at impact energies below 100 keV.

Also shown in Fig. 4 is a calculation by Basko using a semi-classical low-velocity Bohr (LVB) stopping model [37] that extends the Bohr model to lower energies in which the stopping number  $L$  depends on the sign of the projectile. The shape of the LVB curve is similar to that for  $p$  but shifted to higher energies. Besides the  $S^{\bar{p}}$  for H<sub>2</sub> and He measured by Agnello *et al.* the LVB curve is the only one with values larger than for  $p$  impact for energies above the maximum. Below the stopping maximum the LVB results stay well below the  $p$  results and cross all other curves. Besides the position of the stopping maximum the outcome of the LVB method does not fit well any of the curves discussed here.

## IV. DISCUSSION

### A. The Barkas effect

From Eqs. (1) and (2) as well as the discussed experimental evidence it is apparent that higher-order terms in  $Z_p$  will be present in an exact calculation of the stopping power. In order to highlight the Barkas effect and also higher orders of  $L$  in  $S$  it is common to determine the relative stopping power for particles and their antiparticles

$$\frac{\Delta S}{S} = \frac{S^p - S^{\bar{p}}}{S^p}. \quad (20)$$

Using Eqs. (1) and (2) Eq. (20) can be rewritten as

$$\frac{\Delta S}{S} = \frac{2Z_p L_1 + 2(Z_p)^3 L_3 + \dots}{L_0 + Z_p L_1 + (Z_p)^2 L_2 + \dots} \quad (21)$$

showing that it depends only on odd terms. In the case that higher-order terms are insignificant (i.e.,  $|L_{2i+1}| \ll |L_1|$ ,  $i > 0$ )  $\Delta S/S$  becomes approximately proportional to the Barkas term  $L_B$ . Then the first-order correction  $L_B$  can be approximated, using Eqs. (1) and (21), by

$$L_B \approx \sum_{i=0}^{\infty} L_{2i+1} (Z_p)^{2i} = \frac{1}{8\pi(Z_p)^3 Z} v^2 \Delta S. \quad (22)$$

Strictly speaking,  $L_B$  is equal to the correction to the stopping number due to the sum of all odd terms  $L_{2i+1}$  since the projectile charges considered in this work have the absolute value  $|Z_p| = 1$ . Therefore,  $L_B$  can be considered soundly also, if the condition that  $L_1$  is the dominant odd contribution is not fulfilled. Though, in that case it is not appropriate to call  $L_B$  Barkas term.

The present results for  $\Delta S/S$  are shown in Fig. 5(a) for H<sub>2</sub> and He. In order to determine the stopping ratios

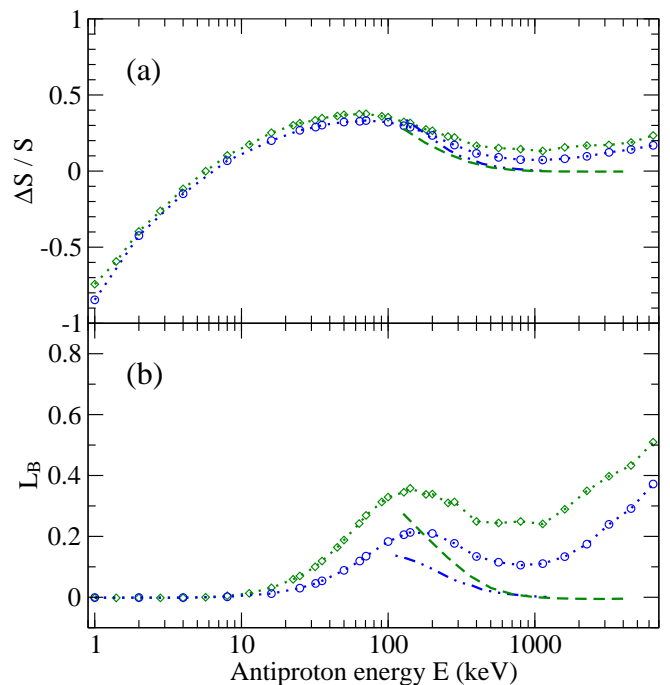


Figure 5: (Color online) (a) Relative stopping power  $\Delta S/S$  for antiprotons and protons colliding with H<sub>2</sub> and He as a function of the impact energy  $E$ . (b) First order correction to the stopping number  $L(E)$  also referred to as Barkas correction  $L_B(E)$  as given in Eq. (22) (see text). Comparison of present  $S^{\bar{p}}$  with experimental  $S^p$  measured by Andersen and Ziegler [32]: green diamonds, H<sub>2</sub> molecule; blue circles, He atom. Comparison of present  $S^{\bar{p}}$  and  $S^p$ : green dashed curve, H<sub>2</sub> molecule; blue dash-doubly-dotted curve, He atom.

the calculations for antiprotons were compared to the experimental data for proton collisions [32]. It can be seen that the ratios for H<sub>2</sub> and He show a comparable behavior. The ratio increases from about  $-0.8$  at 1 keV to a maximal value of approximately 0.35 at 70 keV and then starts to fall off. However, for  $E > 1000$  keV  $\Delta S/S$  begins to increase again for increasing  $E$ . The  $\Delta S/S$  curve for an H atom calculated by Cabrera-Trujillo *et al.* for  $E \leq 300$  keV [22] shows the same qualitative behavior. The outcome from the calculations by Schiwietz *et al.* suggests a decreasing ratio from the stopping maximum until their highest calculated impact energy  $E = 1000$  keV. An increase of the ratio for high energies is not expected since in the limit of high impact energies the first Born approximation is known to give satisfying results.

The calculated  $S^{\bar{p}}$  for H<sub>2</sub> and He are also compared to present results for  $S^p$  for high impact energies in Fig. 5(a). For  $E > 200$  keV the electron capture cross section becomes negligible [43, 44]. Therefore, the employed one-center approach is also capable to describe the stopping of  $p$  for high energies. The relative stopping power  $\Delta S/S$  using only the present data for  $\bar{p}$  and  $p$  impact decreases for increasing  $E$ . This means that the obtained  $S^{\bar{p}}$  results are consistent within the employed model but

deviate slightly from the experimental  $S^p$  data measured by Andersen and Ziegler [32]. In the case that the used experimental proton data are taken as reference that may indicate that the present ratios  $\Delta S / S$  are not sufficiently converged at high energies although the stopping power  $S$  itself compares satisfactory with the experimental results. On the other hand, the present results for  $S^{\bar{p}}$  did not change even with an increase of the energy cutoff by a factor of 20. An even further enlargement of the energy cutoff of the chosen basis set would, however, lead to a drastic increase of the computational time due to the fast oscillating phases in the differential equations for the expansion coefficients  $c_j(\mathbf{R}(t))$  and was therefore not performed.

The present findings for  $L_B$  as given in Eq. (22) are shown in Fig. 5(b) for  $H_2$  and He. The qualitative behavior is similar as for the ratio  $\Delta S / S$  but they differ in the scaling for different  $E$ . Since  $L_B$  is proportional to  $(v)^2$  and therefore to  $E$  it is suppressed at low  $E$  but enhanced at high  $E$ . The difference between  $H_2$  and He is of the order of a factor two. Exactly this factor enters in Eq. (22) as the atomic number  $Z$  in the nominator being one for hydrogen and two for He. For the highest energies  $E > 1000$  keV  $L_B$  determined with the experimental  $S^p$  data increases also with  $E$  due to its proportionality to  $\Delta S / S$ . On the other hand, the  $L_B$  curves evaluated only from the present results for  $S^{\bar{p}}$  and  $S^p$  decrease with increasing  $E$  and, as expected, approach zero for  $E > 1000$  keV. For small energies  $E < 10$  keV  $L_B$  is very small but non zero except for  $E \approx 6$  keV where it changes the sign. However, for these small energies a sizable difference between the stopping power of  $\bar{p}$  and  $p$  exists. This means that the often used condition ( $L_{2i+1} \ll 1$  for  $i \geq 0$ ) to assume that higher-order terms of the stopping number, which lead to different results for particles and antiparticles, are insignificant is not sufficient. While the sum of all odd corrections  $L_B$  already fulfills this condition in Fig. 5(b) for small  $E$  the findings for the stopping power of  $p$  and  $\bar{p}$  impact clearly differ in Figs. 3 and 4.

### B. Excitation energies and ratio $S_{exc}/S_{ion}$

For the correct determination and understanding of the stopping power the different energy-loss processes are of interest. Besides the cross sections for ionization and excitation which are discussed elsewhere (cf. the references in Sec. I) also the energy transfer is of importance. Thereby, quantities like the electron-energy spectra [4] or differential excitation cross sections for transitions into single states [25] provide detailed insight. It is, however, also conclusive to look at the average energies transferred to ionized and bound-excited target atoms. Knowing these quantities it is possible to determine the stopping power out of total cross sections for ionization and excitation.

The average energy transfer to the ionized target atoms or molecules  $\bar{\epsilon}_{ion}$  per electron as a function of the impact

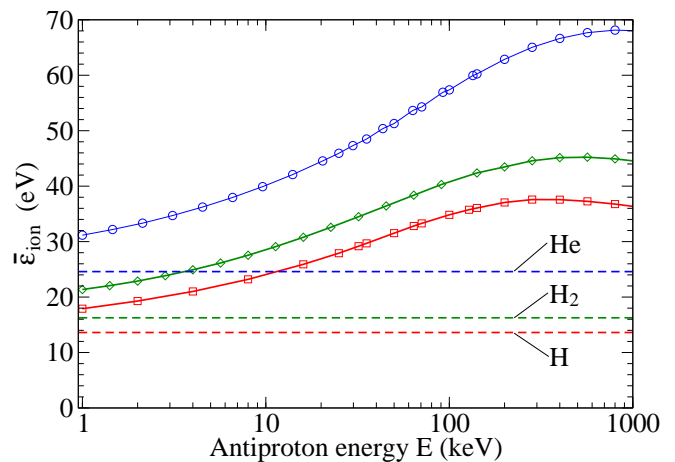


Figure 6: (Color online) The average energy transfer to the ionized electrons  $\bar{\epsilon}_{ion}$  per electron as a function of the  $\bar{p}$  impact energy. Red squares, H atom; green diamonds,  $H_2$  molecule; blue circles, He atom. The ionization potential — being the lower bound — for the three targets are shown as dashed horizontal lines.

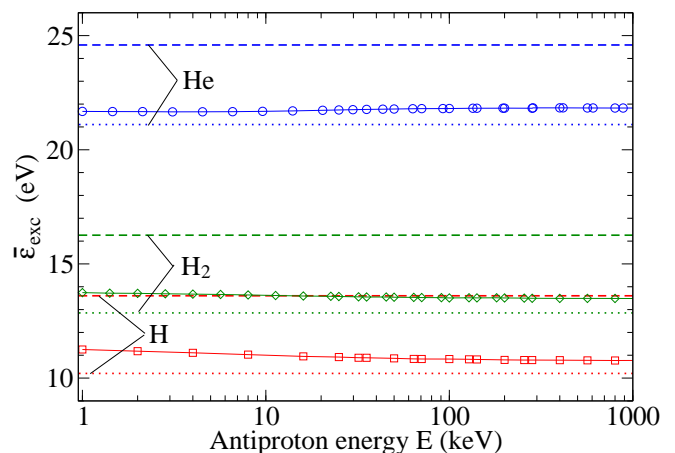


Figure 7: (Color online) The average energy transfer to the bound electrons  $\bar{\epsilon}_{exc}$  per electron as a function of the  $\bar{p}$  impact energy. Red squares, H atom; green diamonds,  $H_2$  molecule; blue circles, He atom. The ionization potentials — upper bound — are shown as dashed horizontal lines and the excitation energy into the lowest dipole-allowed states — lower bound — as dotted horizontal lines.

energy of the projectile  $E$  for the three targets H,  $H_2$ , and He are shown in Fig. 6. Also given are the ionization potentials of the three targets being the lower limit of the energy transfer which is required for ionization. The ionization potentials  $I$  are ordered as  $I^{He} > I^{H_2} > I^H$ . The energy transfer to ionized electrons is ordered in the same way  $\bar{\epsilon}_{ion}^{He} > \bar{\epsilon}_{ion}^{H_2} > \bar{\epsilon}_{ion}^H$ . All  $\bar{\epsilon}$  increase for increasing impact energy  $E$ . This trend is in agreement with the previous analysis of the electron-energy spectra for  $H_2$  [4, 29]. The increasing importance of the higher-lying

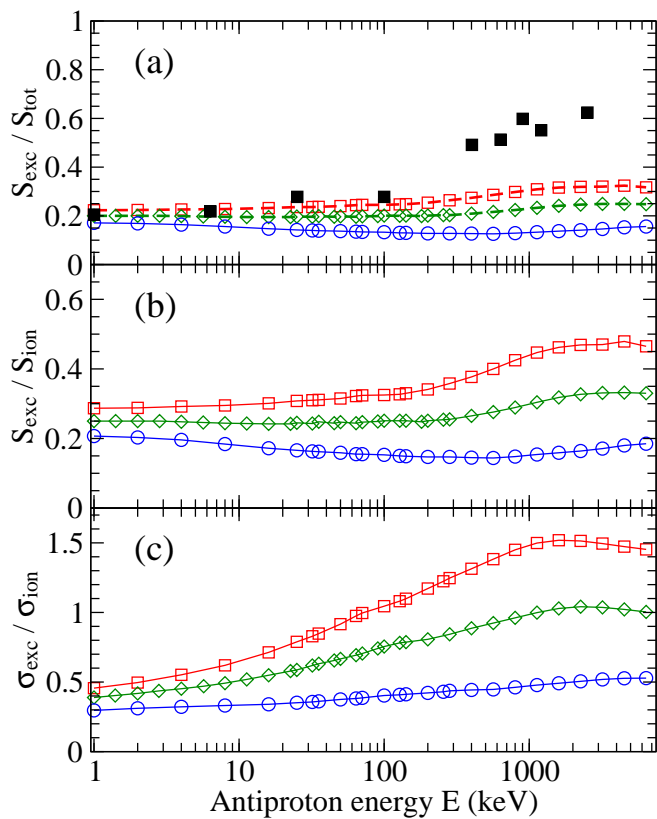


Figure 8: (Color online) Ratios of the stopping power as a function of the  $\bar{p}$  impact energy. (a) Ratio of stopping power due to excitation  $S_{\text{exc}}$  and total stopping power  $S_{\text{tot}} = S$ . (b) Ratio of  $S_{\text{exc}}$  and stopping due to ionization  $S_{\text{ion}}$ . (c) Ratio of cross sections for excitation  $\sigma_{\text{exc}}$  and ionization  $\sigma_{\text{ion}}$ . Present data: red squares, H atom; green diamonds,  $\text{H}_2$  molecule; blue circles, He atom. Custidiano and Jakas [23]: black filled squares, H atom with CTMC.

unbound states requires on the other hand also a sufficient description of the continuum states at large electron energies  $\epsilon$ . It turned out that the results for large  $E$  become sensitive to the energy cutoff of the employed basis set. Therefore, it is important at high impact energies  $E$  to extend the continuum part of the basis with continuum states belonging to higher electron energies  $\epsilon$  in order to achieve convergence.

The average energy transfer to the excited atoms or molecules  $\bar{\epsilon}_{\text{exc}}$  shown in Fig. 7 is on the other hand only weakly dependent on the impact energy  $E$ . The  $\bar{\epsilon}_{\text{exc}}$  curves for the three targets are energetically ordered in the same way as the  $\bar{\epsilon}_{\text{ion}}$ . Also given in Fig. 7 are the ionization potentials being the upper limits for bound state transitions as well as the minimum energy transfer into the first excited states for the three targets which are all independent of  $E$ . The  $\bar{\epsilon}_{\text{exc}}$  curves for all three targets stay close to the minimum lines for all  $E$ . This is in accordance to the fact that the first excited dipole-allowed state is the dominant excitation channel as was observed in [4, 27, 29] and is in agreement with measurements for

$e^- + \text{H}_2$  collisions [45]. For decreasing  $E$  the contribution of the higher excited states increases for H and  $\text{H}_2$  while it decreases slightly in the case of He.

In Fig. 8 the relative contribution to the stopping power due to ionization and excitation is considered according to the Eqs. (17) and (18). The relative importance of both processes excitation and ionization, depends on the target and the impact energy of the  $\bar{p}$ . In general it can be concluded that in the whole energy range the energy loss due to ionization dominates the loss due to excitation as can be seen in Fig. 8(b). This is in contrast to the findings for alkali-metal atoms where the  $\bar{p}$  loses energy mainly due to the bound-state excitation [28].

The fraction of energy which goes into excitation given in Fig. 8(a) is largest for H and smallest for He in accordance with the corresponding ratios of excitation to ionization cross section shown in 8(c). This may be linked to the ionization potential which is smallest for H and largest for He.

The present ratio  $S_{\text{exc}}/S_{\text{tot}}$  for H atoms agrees with the findings by Custidiano and Jakas [23] in Fig. 8(a) for low energies and is still comparable for  $E \leq 100$  keV. Their statement that  $S_{\text{exc}}/S_{\text{tot}}$  is approximately a monotonously increasing function with  $E$  up to their largest  $E = 2.5$  MeV is also in accordance with the present findings. For  $E > 300$  keV, however, their ratio lies clearly above the present results. This is in contrast to what was observed for the total stopping power in Fig. 2 where the results by Custidiano and Jakas agreed with the present findings for high energies but disagreed for low energies. Regarding these differences one may conclude that although the total results are in agreement for high energies the underlying physics seems not to be described correctly in one of the calculations. As has been seen when considering the electron-energy spectra [4] as well as the convergence of  $\bar{\epsilon}_{\text{ion}}$  high-energy electronic states become more important for increasing  $E$ . An energy cutoff for the electrons needed in any numerical treatment has to be chosen carefully in order to obtain a converged  $S_{\text{ion}}$  as shown in Fig. 1 and table I. If the energy cutoff is not sufficiently large, the  $\bar{\epsilon}_{\text{ion}}$  becomes too small which finally leads to a ratio  $S_{\text{exc}}/S_{\text{tot}}$  that is too large. This trend was observed in the present convergence studies.

### C. Comparison of $S$ for H, $\text{H}_2$ , and He

In Fig. 9 the present stopping power curves for all three targets H,  $\text{H}_2$ , and He are shown in one graph. For comparison also the experimental data for  $\bar{p}$  and  $\mu^-$  impact on  $\text{H}_2$  and He targets are given. In the limit of high energies  $E > 500$  keV the present results for atomic and molecular hydrogen coincide which is also obvious from Table II. For these energies the present findings for He stay clearly above those for hydrogen. For  $E > 2000$  keV, however, the present  $S$  curve for He approaches the

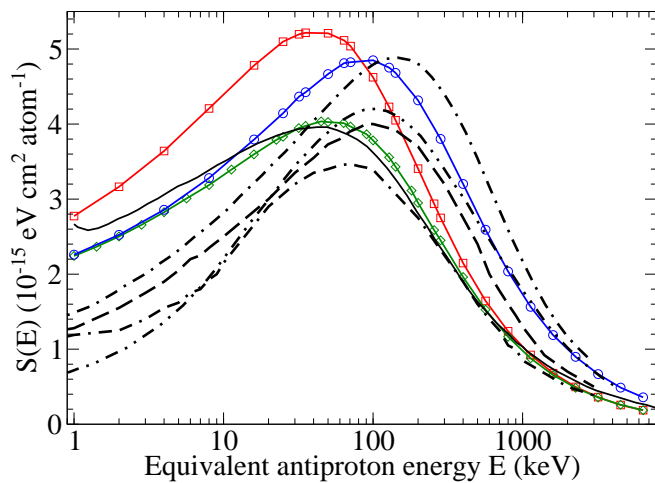


Figure 9: (Color online) Comparison of the energy loss cross sections  $S(E)$  for H, H<sub>2</sub>, and He targets as a function of the equivalent antiproton impact energy  $E$ . **Theory.** Present results: red solid curve with squares, H; green solid curve with diamonds, H<sub>2</sub>; blue solid curve with circles, He. **Experiment.** H<sub>2</sub>: black solid curve, Adamo *et al.* [11],  $\bar{p}$ ; black dashed curve, Agnello *et al.* [12],  $\bar{p}$ ; black doubly-dash-dotted curve, Hauser *et al.* [18],  $\mu^-$ . He: black dash-dotted curve, Agnello *et al.* [12],  $\bar{p}$ ; black dash-doubly-dotted curve, Kottmann [17],  $\mu^-$ .

hydrogen results multiplied by two (cf. Table II).

The high-energy behavior can be made plausible by considering how the impact parameter region — and therefore also the distance  $r$  between the electron and the nucleus — where the main contribution to the energy loss originates from depends on the projectile energy. It is known that for large impact energies the relative importance of distant encounters for the electronic stopping power is increasing. The used model potential in Eq. (8) fulfills the requirement that it behaves for  $r \rightarrow \infty$  as the potential of a hydrogen atom. Since at large distances the outer electron of the H<sub>2</sub> molecule and He atom is practically only exposed to the field of the sum of the three remaining charges, the same stopping power for hydrogen atoms and molecules *per atom* can be expected. A similar argument can be applied in the case of the stopping power of alkali-metal atoms in the case that only the valence electrons are considered. They show the same behavior for large impact energies [28] due to the fact that they also have a hydrogen-like potential at large  $r$ . However, the alkali stopping power coincides with the hydrogen results only for higher energies  $E > 4000$  keV for Na, K, and Rb and  $E > 1000$  keV for Li since the alkali-metal atoms are spatially more extended than hydrogen.

The doubled values for He for large  $E$  can be understood in the following way. For high impact velocities the collision process can be considered independently for both electrons of the He atom since the projectile-electron interaction happens on a much shorter time scale than the mean electron motion and finally, the *dy-*

*amic* electron-electron interaction only plays a minor role. Therefore, in the high-energy regime it is also meaningful to consider the stopping power per *electron* instead of per *atom* leading then to the same result for H, H<sub>2</sub>, and He targets.

At low energies the present stopping power curves for H<sub>2</sub> and He coincide. For energies around and below the stopping maximum the results for hydrogen atoms obviously differ from those for the molecules lying clearly above the He and H<sub>2</sub> curves. This could have been expected since all previous attempts to compare calculated  $S$  data for H atoms with experimental curves for H<sub>2</sub> turned out to be not satisfactory. The apparent differences were ascribed to *molecular* effects [21–23] but were not further specified. A full treatment of the H<sub>2</sub> molecule has to account for a two-center description with two interacting electrons and vibrational and rotational motion of the nuclei. This leads, e.g., to a different ionization potential and an asymmetry of the charge distribution compared to an H atom, dynamic two-electron effects as well as the existence of different rotational and vibrational states. The present calculations employ an atomic-like one-center model for the description of H<sub>2</sub>. It provides an appropriate ionization potential which is, however, static since the second electron is accounted for by a screening potential which does not allow for dynamic interaction effects. The nuclear motion is to a certain extent included using the linearity of the antiproton cross sections in  $R_n$ . The present findings seem to show that the cross sections and therefore also the stopping power are strongly determined by the correct ionization potential of the target. Thereby, ionization is the main energy loss channel for  $\bar{p}$  collisions with H<sub>2</sub>. Specific molecular effects due to the existence of two centers like rotational and vibrational motion of the nuclei, dissociation or an asymmetric charge distribution seem to play a minor role for impact energies above the stopping maximum. On the other hand, dynamic electron-electron effects during the collision which are excluded in the present approach seem to become important for energies below the stopping maximum due to the fact that (i) the longer time scales allow for interactions between the electrons and (ii) the inelastic collisions take place closer to the nuclei where the electron density is higher.

## V. CONCLUSION

Time-dependent close-coupling calculations of the electronic stopping power for antiproton collisions with atomic and molecular hydrogen as well as helium have been performed in an impact-energy range from 1 keV to 6.4 MeV. The collision process is described using the classical trajectory approximation. The H, H<sub>2</sub>, and He targets are treated as (effective) one-electron systems employing a model potential which provides the correct ground-state ionization potentials. It can be used for different fixed internuclear distances in the case of H<sub>2</sub> and

behaves like the pure Coulomb potential of a hydrogen atom for large  $r$ .

Calculations for the stopping power of hydrogen which distinguish between atomic and molecular targets are presented and discussed considering the existing theoretical and experimental literature, respectively. The present He results are considered together with theoretical and experimental results. The stopping power for H compares well with other non-perturbative calculations while the He and H<sub>2</sub> data give a good qualitative insight but seem to overestimate  $S$  for low impact energies. This might be caused by the static description of the second electron using an effective one-electron model. For high energies the present H<sub>2</sub> and He results agree with measurements by Adamo *et al.* [11] and for  $\mu$  impacts by Kottmann *et al.* [17, 18] but disagree with the findings by Agnello *et al.* [12] which lie above the proton stopping power. For the highest energies  $E > 2$  MeV the present results for  $S$  coincide for all three targets, if the stopping power is considered per electron instead of per atom as usually done. This means, in the case of fast  $\bar{p}$  the electrons can be interpreted as independent particles and that the interaction takes place mainly at large impact parameters where all electrons experience the same potential.

The energy loss of the projectile is for all three tar-

gets mainly caused by ionization of electrons in contrast to alkali-metal atom targets for which excitation is the dominant loss process. While the average energy transferred to excited target atoms is only weakly dependent on  $E$ , the average energy transferred to the ionized targets increases with  $E$ . Therefore, the calculations at high energies are computationally more demanding since a basis including high-lying continuum states is required.

In order to improve the description of the stopping power below the maximum a two-electron description of the H<sub>2</sub> and He targets shall be implemented. This would drastically reduce the uncertainties still persisting at low impact energies and present a stringent test of the accuracy of the  $\bar{p}$  measurements of the stopping power but in turn also for the ionization and excitation cross sections of  $\bar{p}$  collisions with He and H<sub>2</sub>.

## ACKNOWLEDGMENTS

The authors would like to acknowledge helpful discussions with Prof. Knudsen and Prof. Kottmann. The authors also want to thank Prof. Schiwietz and Prof. Lodi Rizzini for correspondence. The authors are grateful to BMBF (FLAIR Horizon) and *Stifterverband für die deutsche Wissenschaft* for financial support.

- 
- [1] H. Knudsen, H.-P. Kristiansen, H. Thomsen, U. Uggerhøj, T. Ichioka, S. Møller, N. Kuroda, Y. Nagata, H. Torii, H. Imao, et al., *Phys. Rev. Lett.* **101**, 043201 (2008).
  - [2] P. Hvelplund, H. Knudsen, U. Mikkelsen, E. Morenzoni, S. P. Møller, E. Uggerhøj, and T. Worm, *J. Phys. B* **27**, 925 (1994).
  - [3] A. M. Ermolaev, *Hyperfine Interact.* **76**, 335 (1993).
  - [4] A. Lühr and A. Saenz, *Phys. Rev. A* **78**, 032708 (2008).
  - [5] H. Bethe, *Ann. Phys.* **5**, 325 (1930).
  - [6] H. Bethe, *Z. Phys.* **76**, 293 (1932).
  - [7] W. H. Barkas, J. N. Dyer, and H. H. Heckman, *Phys. Rev. Lett.* **11**, 26 (1963).
  - [8] J. Lindhard, *Nucl. Instrum. Methods* **132**, 1 (1976).
  - [9] L. H. Andersen, P. Hvelplund, H. Knudsen, S. P. Møller, J. O. P. Pedersen, E. Uggerhøj, K. Elsener, and E. Morenzoni, *Phys. Rev. Lett.* **62**, 1731 (1989).
  - [10] S. P. Møller, A. Csete, T. Ichioka, H. Knudsen, U. I. Uggerhøj, and H. H. Andersen, *Phys. Rev. Lett.* **88**, 193201 (2002).
  - [11] A. Adamo, M. Agnello, F. Balestra, G. Belli, G. Bendiscioli, A. Bertin, P. Boccaccio, G. C. Bonazzola, T. Bressani, M. Bruschi, et al., *Phys. Rev. A* **47**, 4517 (1993).
  - [12] M. Agnello, G. Belli, G. Bendiscioli, A. Bertin, E. Botta, T. Bressani, M. Bruschi, M. P. Bussa, L. Busso, D. Calvo, et al., *Phys. Rev. Lett.* **74**, 371 (1995).
  - [13] E. Lodi Rizzini, A. Bianconi, M. P. Bussa, M. Corradini, A. Donzella, L. Venturelli, M. Bargiotti, A. Bertin, M. Bruschi, M. Capponi, et al., *Phys. Rev. Lett.* **89**, 183201 (2002).
  - [14] E. Lodi Rizzini, A. Bianconi, M. Bussa, M. Corradini, A. Donzella, M. Leali, L. Venturelli, N. Zurlo, M. Bargiotti, A. Bertin, et al., *Phys. Lett. B* **599**, 190 (2004).
  - [15] A. Bianconi, M. Corradini, A. Cristiano, M. Leali, E. Lodi Rizzini, L. Venturelli, N. Zurlo, and R. Donà, *Phys. Rev. A* **78**, 022506 (2008).
  - [16] E. Lodi Rizzini, private communication (2008).
  - [17] F. Kottmann, in *Proc. 2nd Int. Symp. on Muon and Pion Interactions with Matter*, edited by V. P. Dzelepov (Dubna, 1987), p. 268.
  - [18] P. Hauser, F. Kottmann, C. Lüchinger, and R. Schaeren, in *Muonic atoms and molecules*, edited by L. A. Schaller and C. Petitjean (Basel, 1993), p. 235.
  - [19] F. Kottmann, in *Proc. Int. School of Physics of Exotic Atoms*, edited by C. Rizzo and E. Zavattini (Trieste, 1994), p. 297.
  - [20] R. Schmidt, H. Daniel, F. Hartmann, P. Hauser, F. Kottmann, M. Mühlbauer, C. Petitjean, W. Schott, D. Taquu, and P. Wojciechowski, *Euro. Phys. J. D* **3**, 119 (1998).
  - [21] G. Schiwietz, U. Wille, R. D. Muiño, P. D. Fainstein, and P. L. Grande, *J. Phys. B* **29**, 307 (1996).
  - [22] R. Cabrera-Trujillo, J. R. Sabin, Y. Öhrn, and E. Deumens, *J. Phys. B* **71**, 012901 (2005).
  - [23] E. R. Custidiano and M. M. Jakas, *Phys. Rev. A* **72**, 022708 (2005).
  - [24] J. S. Cohen, *Phys. Rev. A* **27**, 167 (1983).
  - [25] A. Lühr, Y. V. Vanne, and A. Saenz, *Phys. Rev. A* **78**, 042510 (2008).
  - [26] A. Bertin, M. Bruschi, M. Capponi, I. D'Antone, S. De Castro, A. Ferretti, D. Galli, B. Giacobbe, U. Marconi, M. Piccinini, et al., *Phys. Rev. A* **54**, 5441 (1996).
  - [27] A. Lühr and A. Saenz, *Phys. Rev. A* **77**, 052713 (2008).
  - [28] A. Lühr, N. Fischer, and A. Saenz, *Hyperfine Interact.*

- (2009).
- [29] A. Lühr and A. Saenz, *Hyperfine Interact.* (2009).
- [30] Y. V. Vanne and A. Saenz, *J. Mod. Opt.* **55**, 2665 (2008).
- [31] A. Saenz and P. Froelich, *Phys. Rev. C* **56**, 2162 (1997).
- [32] H. H. Andersen and J. F. Ziegler, *Hydrogen Stopping Powers and Ranges in All Elements* (Pergamon, New York, 1977).
- [33] W. Kolos and L. Wolniewicz, *J. Chem. Phys.* **41**, 3674 (1964).
- [34] L. H. Andersen, P. Hvelplund, H. Knudsen, S. P. Møller, J. O. P. Pedersen, S. Tang-Petersen, E. Uggerhøj, K. Elsener, and E. Morenzoni, *J. Phys. B* **23**, L395 (1990).
- [35] H. Knudsen, private communication (2008).
- [36] L. A. Wehrman, A. L. Ford and J. F. Reading, *J. Phys. B* **29**, 5831 (1996).
- [37] M. M. Basko, *Eur. Phys. J. D* **32**, 9 (2005).
- [38] P. D. Fainstein, V. H. Ponce, and R. D. Rivarola, *Phys. Rev. A* **36**, 3639 (1987).
- [39] L. H. Andersen, P. Hvelplund, H. Knudsen, S. P. Møller, J. O. P. Pedersen, S. Tang-Petersen, E. Uggerhøj, K. Elsener, and E. Morenzoni, *Phys. Rev. A* **41**, 6536 (1990).
- [40] M. Foster, J. Colgan, and M. S. Pindzola, *Phys. Rev. Lett.* **100**, 033201 (2008).
- [41] A. Igarashi, S. Nakazaki and A. Ohsaki, *Nuc. Instrum. Methods Phys. Res. B* **214**, 135 (2004).
- [42] J. F. Reading, T. Bronk, A. L. Ford, L. A. Wehrman, and K. A. Hall, *J. Phys. B* **30**, L189 (1997).
- [43] M. B. Shah and H. B. Gilbody, *J. Phys. B: At. Mol. Phys.* **18**, 899 (1985).
- [44] R. Shingal and C. D. Lin, *Phys. Rev. A* **40**, 1302 (1989).
- [45] X. Liu, D. E. Shemansky, S. M. Ahmed, G. K. James, and J. M. Ajello, *J. Geophys. Res.* **103**, 26739 (1998).